Progress In Electromagnetics Research Letters, Vol. 104, 37–46, 2022

Small Formfactor Phased Array for Simultaneous Spatial and Channel Diversity Communications

Daniel Guidotti[1, *], Binbin Yang[2], Muhammad S. Omar[1], Shang-Jen Su[1], Yahya M. Alfadhli[1], Gee-Kung-Chang[1], and Xiaoli Ma[1]

Abstract—A high frequency device design and simulation results are reported for an 8×8 phased array of unit cells. Each unit cell comprises a (3×3) sub-array of 1/4 wave rod monopole radiators. Each unit cell is the basic building block that can be arranged to form 9 interpenetrating arrays. Each interpenetrating array comprises an independently addressable 8×8 array of 1/4 wave rod monopole radiators that fits into the lateral space of a single 8×8 array of patch radiators but can operate on 9 independent radio frequency channels within the same contiguous communication band without interference and can direct each radio frequency channel into independent directions simultaneously. The beamformer architecture, operation principle, and simulation results are presented and discussed, and an outline of its construction based on 2.5D integration is presented.

1. INTRODUCTION

This work was undertaken as a means to provide a hardware-based solution to the persistently increasing value of the "peak to average power ratio" (PAPR) with increasing number of subcarriers, M, in communication systems using multicarrier modulation, particularly "orthogonal frequency division multiple access" (OFDMA) communication [1, 2] via a MIMO air interface which remains as the main workhorse of 5.5G and 6G mobile communication for the foreseeable future.

The initial goals were as follows:

- Keep the number of subcarriers, M, as low as practical and
- Compensate for the lower throughput by a commensurate or greater increase in the number of transmitted OFDMA channels without increasing the air interface formfactor and keeping hardware complexity as low as possible by means of 2.5D passive interposer integration.

To this end, this work initially aimed at large outdoor base station phased array panels, each composed of (3×3) sub-arrays unit cells comprising 1/4 wave rod monopole radiators arranged in (8×8) unit cells to form one of 9 interpenetrating phased arrays operating in the millimeter wave spectrum. This provides 9 independently addressable phased arrays in the same formfactor as a single (8×8) phased array of patch radiators.

Smaller phased arrays may be used in smaller base stations suitable for indoor venues such as conventions, technology fairs, and trade shows.

This paper describes how to construct a sub-array unit cell containing $N \times N$ high aspect ratio 1/4 wave rod monopole radiators as the basic building unit to construct $N \times N$ interpenetrating,

Received 5 March 2022, Accepted 26 April 2022, Scheduled 11 May 2022

* Corresponding author: Daniel Guidotti (guidotti.daniel@gmail.com).

[1] School of Electrical and Computer Engineering, Georgia Institute of Technology, 777 Atlantic Drive, Atlanta, GA 30332-0001, USA. [2] Department of Electrical and Computer Engineering, North Carolina A&T State University, 1601 E. Market Street, Greensboro, NC 27411, USA.

independently addressable phased arrays, each containing $(I \times J)$ 1/4 wave rod monopoles within the formfactor of a legacy $(I \times J)$ patch array that can only operate as a single phased array.

Further, each interpenetrating array may be spectrally guarded by a narrow bandpass filter with, for example, a center frequency f_0 at 30 GHz, a 200 MHz passband, and 50 dB/MHz roll-off. Thus, each of $N \times N$ interpenetrating arrays of size $(I \times J)$ can independently direct each channel in desired directions and all within a formfactor of a comparable array of $(I \times J)$ patch radiators. The advantages offered by 1/4 wave rod monopole radiator beamformers are:

- A sub-array of $N \times N$ 1/4 wave rod monopole radiators can easily fit in a unit cell that would otherwise house only one patch radiator. This singular distinction and the commercial availability of narrow bandpass, high rejection roll-off rectangular waveguide bandpass filters enable the development of high channel density, small formfactor base stations air interfaces.
- Consequently, $(I \times J)$ interpenetrating, 1/4 wave, rod monopole phased arrays, each with independent spatial and channel diversity, can coexist in the lateral space that would otherwise be used by a single patch beamformer operating on a single radio frequency (RF) channel.

It is noted that the distribution of the $N \times N$ monopoles in a sub-array unit cell and their relative separation is largely inconsequential, bar electrical isolation. RF coherence in each interpenetrating phased array attains at the inter-unit cell separation. Intra sub-array unit cell monopole separation is substantially inconsequential.

2. ARCHITECTURE, SCALABILITY AND TAXONOMY OF THE 1/4 WAVE ROD MONOPOLE MULTICHANNEL PHASED ARRAY

Figure 1 depicts a sub-array unit cell containing a substrate insulator, a ground plane, and a 3×3 sub-array lattice of 1/4 wave rod monopole radiators equally spaced at intervals $(\Delta x, \Delta y)$ along the indicated X and Y directions. Each monopole is located at a unique point on the sub-array lattice designated by three numbers, for example, (3, 1, 3), where the first number designates the unit cell, and the following two numbers designate the X, Y locations of the rod monopole in a plane parallel to the ground plane of the sub-array.

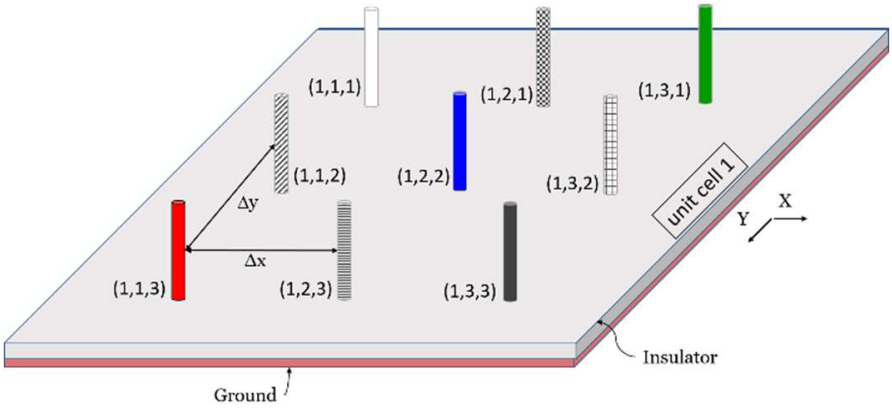

Figure 1. Unit cell containing an $(N \times N) = (3 \times 3)$ sub-array lattice of 1/4 wave rod monopoles insulated from a ground plane.

Monopoles in Fig. 1 at coordinates (1, 1, 3), (1, 2, 2), and (1, 3, 1) are designated as cardinal monopoles as they, and other similarly located monopoles in other unit cell sub-arrays, are of special interest in the beamforming simulations as discussed in Section 3. A number of unit cells, similar to that depicted in Fig. 1, may be arranged in contiguous 2-D arrays. For example, Fig. 2 depicts an array, $(I \times J) = (2 \times 2)$, of similar unit cells.

Rules for constructing interpenetrating phased arrays of monopole radiators:

i) each monopole is used as a radio frequency radiator.

ii) spacings Δx and Δy are substantially less than the RF coherence length.

iii) only one monopole in each unit cell sub-array can partake in only one of $I \times J$ interpenetrating phased arrays.

iv) only monopoles located at the same coordinates in adjacent unit cells can form an interpenetrating phased array.

v) only corresponding points in adjacent sub-array unit cells can be within the RF coherence length.

vi) each radiator may be offset by a phase delay (ϑ_x, φ_y), as depicted in Fig. 2, relative to a radiator located at a corresponding point in the sub-array lattice of an adjacent unit cell.

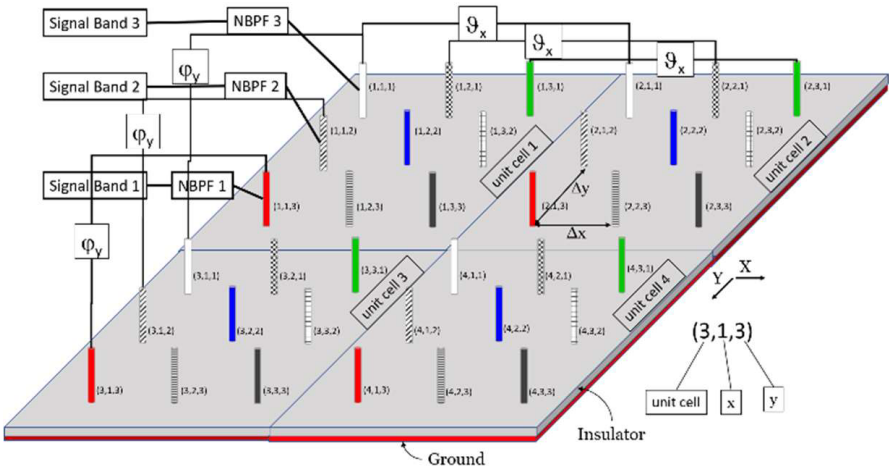

Figure 2. An $I \times J = 2 \times 2$ array of unit cells, each containing an $N \times N = 3 \times 3$ sub-array lattice of 1/4 wave rod monopoles. A relative phase shift between adjacent monopoles in x, y rows in adjacent sub-arrays is indicated by ϑ_x, φ_y.

The 2×2 unit cell array in Fig. 2 constitutes 9, 2×2 interpenetrating arrays, each comprising 4 monopoles, one monopole from each lattice point in each of the 4 sub-array unit cells. Monopoles in Fig. 2, located at the cardinal coordinates (1, 2, 2), (3, 2, 2), (2, 2, 2), and (4, 2, 2) in corresponding sub-array lattices are designated as **"center" blue monopoles**; those located at (1, 1, 3), (3, 1, 3), (2, 1, 3), and (4, 1, 3) as **"outer edge" red monopoles**, while those located at (1, 3, 1), (3, 3, 1), (2, 3, 1), and (4, 3, 1) as **"inner edge" green monopoles**.

An array $(I \times J)$ of unit cells formed in the manner described above is termed an interpenetrating phased array because precisely each of its constituent rod monopole radiators belongs to one of the $(N \times N)$ unit cell sub-arrays of rod radiators that are shared among each of the $(I \times J)$ interpenetrating phased arrays. For example, in Fig. 2, if a relative phase shift, φ_y, is applied between (unit-cell-wise) adjacent monopoles in all "y" rows in the entire array of unit cells and, similarly, if a relative phase shift, ϑ_x, is applied between (unit-cell-wise) adjacent monopoles in all "x" rows in the entire array of unit cells, then coherent RF emission can be made to occur at a desired beam angle of elevation above the ground plane and at a desired azimuth angle in the said plane. As depicted in Fig. 2, three of the nine interpenetrating arrays are seen to carry a signal channel as depicted by "Signal Bands 1–3" and "Narrow Bandpass Filters 1–3." Only three of nine channels are so depicted to avoid drawing conjestion.

In a further note, scaling the number of unit cells, while keeping constant the number of monopoles per unit cell, scales the spatial resolution and gain of each $I \times J$ interpenetrating array, while scaling the number of radiators per unit cell scales the number of independent RF channels. Here, an RF channel is defined by a center frequency and bandwidth. It is assumed that sufficiently narrow bandpass filters with sufficiently steep rolloff are commercially available (see Section 6) so as to isolate each subarray. Of course, increasing the number of unit cells in an array and/or increasing the number of radiators per unit cell will increase both complexity and power dissipation. A unit cell with high radiator density can only be achieved with high aspect ratio RF radiators.

3. SIMULATION PROTOCOL AND RESULTS

All simulations were conducted on Ansys 2021/R2 HFSS Electronic Desktop simulator at 30 GHz ($\lambda = 10$ mm) using coaxial coupling to radiating elements despite probe access holes in the ground plane and wave port excitation.

Fig. 3 shows an HFSS model image of a 3×3 sub-array lattice of rod monopoles having 0.1 mm radius and 2.5 mm height above the ground plane ($1/4\lambda$ at 30 GHz) and equally spaced on 1.5 mm centers. The sub-array lattice has a conducting shield wall of circumvallation approximately $1/5\lambda$ in height and functions as a radiation equalizer which equalizes the RF gain for each sub-array, irrespective of monopole coordinate provenance in a unit cell. Without the shield wall, main lobes emanating from an interpenetrating phased array composed of monopoles located at the center of each 3×3 sub-array (Figs. 1, 2) appear symmetrical, while main lobes emanating from an interpenetrating array composed

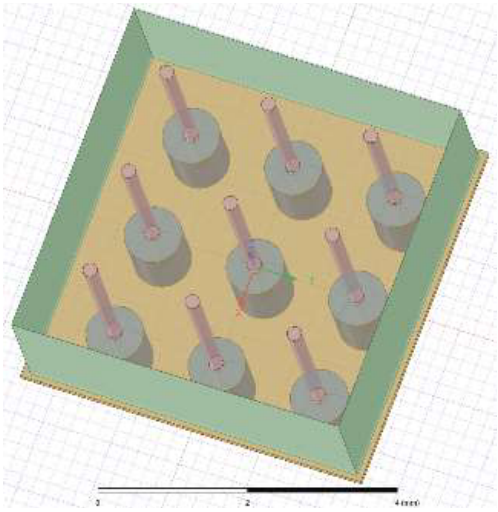

Figure 3. Model unit cell containing a 3×3 sub-array of 1/4 wave rod monopoles. Substrate: Rogers RT/duroid®5880 Laminate, size: $5 \times 5 \times 0.1\,\text{mm}^3$. Monopole radiators on 1.5 mm centers above a ground plane. Coax feeds are below the ground plane. Contact to monopole is through a hole in the ground plane. Conducting shield wall of circumvallation is approximately $1/5\lambda$ tall.

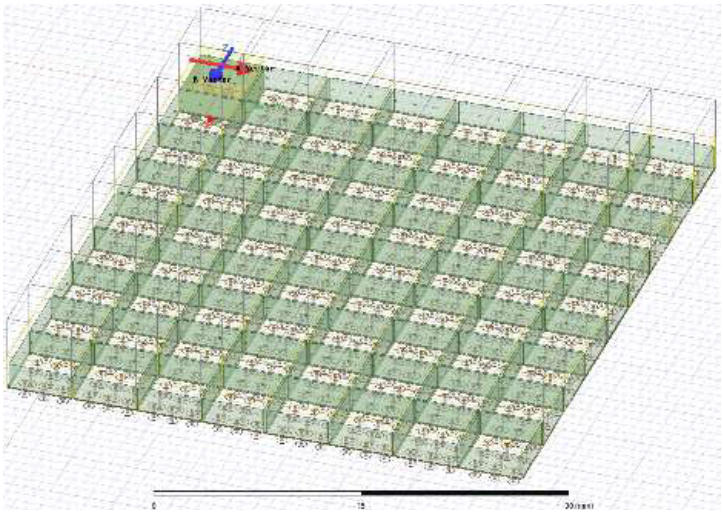

Figure 4. HFSS model image of an 8×8 array of unit cells, each comprising 3×3 sub-array of $1/4\lambda$ rod monopole radiators. Total of 576 radiators.

of monopoles located at corresponding corners such as (1, 3, 1) or (1, 1, 3) of each 3×3 sub-array appear asymmetrical (not shown here).

Fig. 4 shows an HFSS model image of an 8×8 array of unit cells, each containing a 3×3 sub-array of monopole radiators within a conductive shield wall of circumvallation (Fig. 3). The 3×3 rod monopole arrays form 9 independent interpenetrating arrays (as in Fig. 2) corresponding to 9 interpenetrating arrays, while occupying approximately the same in-plane area as a patch array that can only operate on a single channel (see Section 4).

Monopole Array Simulation Results — Total Directivity (dB):

A. Figures 5 and 6 show the emission patterns for a $(3 \times 3) \times (8 \times 8)$ *MONOPOLE ARRAY when the* ***Center Monopole is Active****.*

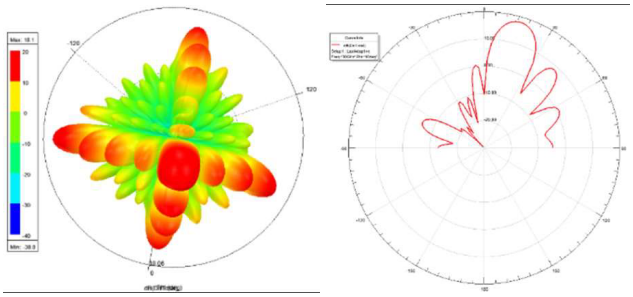

Figure 5. $(3 \times 3) \times (8 \times 8)$ Center Active; 15° Elevation; 15° Azimuth.

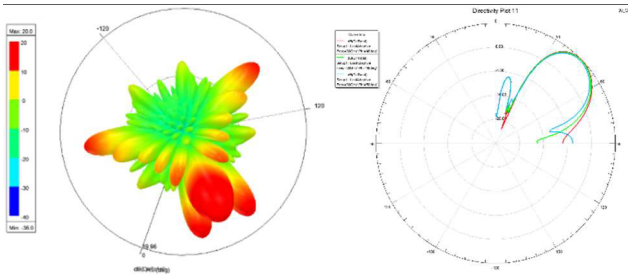

Figure 6. $(3 \times 3) \times (8 \times 8)$ Center Active; 45° Elevation; 45° Azimuth.

B. Figures 7 and 8 show the emission patterns for a $(3 \times 3) \times (8 \times 8)$ *MONOPOLE ARRAY when the* ***Outer Edge Monopole is Active****.*

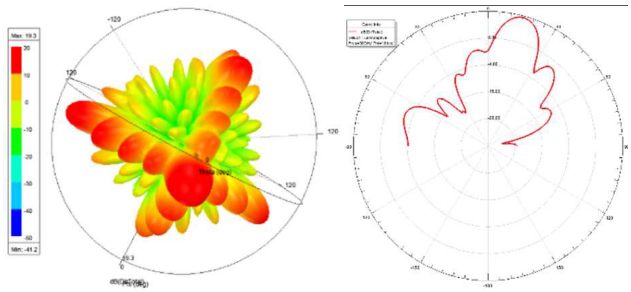

Figure 7. $(3 \times 3) \times (8 \times 8)$ Outer Edge Active; 15° Elevation; 15° Azimuth.

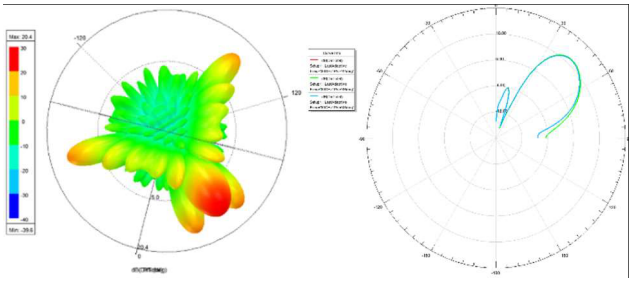

Figure 8. $(3 \times 3) \times (8 \times 8)$ Outer Edge Active; 45° Elevation; 45° Azimuth.

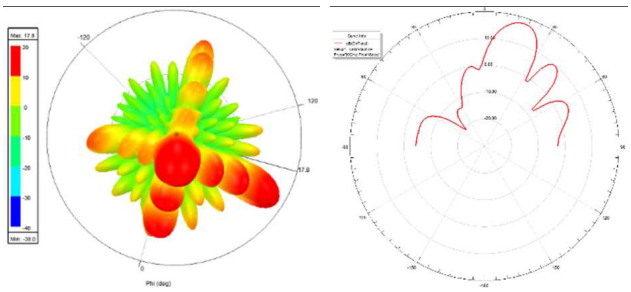

Figure 9. $(3 \times 3) \times (8 \times 8)$ Inner Edge Active; 15° Elevation; 15° Azimuth.

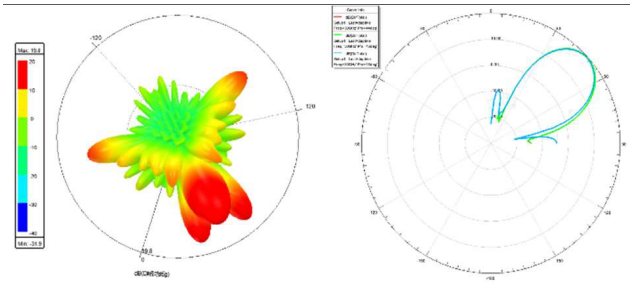

Figure 10. $(3 \times 3) \times (8 \times 8)$ Inner Edge Active; 45° Elevation; 45° Azimuth.

C. Figures 9 and 10 show the emission patterns for a $(3 \times 3) \times (8 \times 8)$ *MONOPOLE ARRAY when the* ***Inner Edge Monopole is Active****.*

4. COMPARISON WITH AN 8×8 ARRAY OF PATCH RADIATORS

For reference, we present similar results for an 8×8 array of patch radiators. The HFSS model of one patch is shown in Fig. 11.

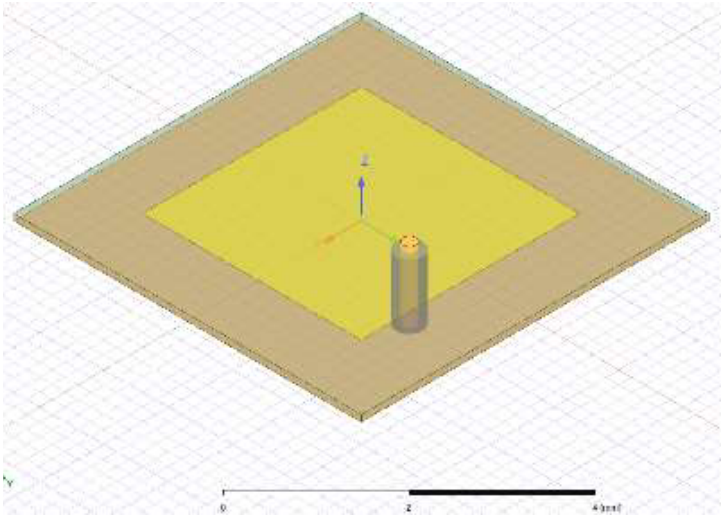

Figure 11. Patch unit cell; size: $3.4 \times 3.4\,\mathrm{mm}^2$. Coax probe offset: $y = 0.75\,\mathrm{mm}$. Substrate: Rogers RT/duroid®5880. Laminate size: $5.4 \times 5.4 \times 0.1\,\mathrm{mm}^3$.

Patch Array Simulation Results — Total Directivity (dB):

Figures 12 and 13 show the emission patterns for an (8×8) *ARRAY of PATCH radiators.*

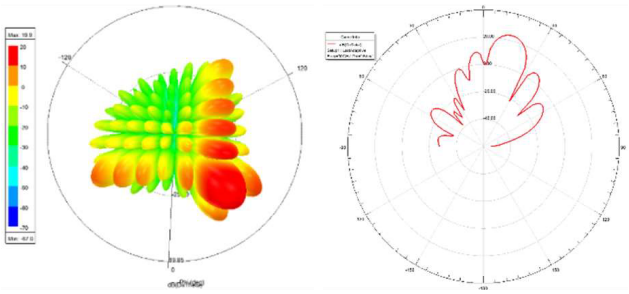

Figure 12. 8×8 Patch Array; 15° Elevation; 15° Azimuth.

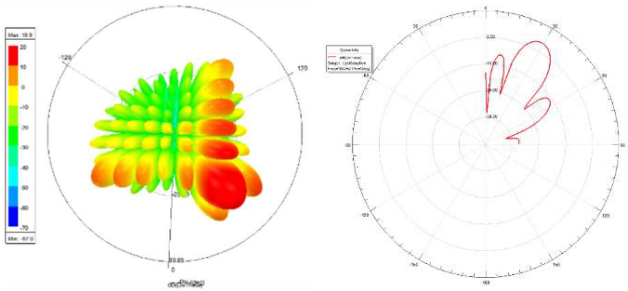

Figure 13. 8×8 Patch Array; 45° Elevation; 45° Azimuth.

Additional insight can be obtained by comparing directivity gains as seen in side-by-side rectangular plots for far field emissions from 8×8 patch radiator arrays and 8×8 interpenetrating arrays or rod monopole radiators introduced in this paper. Figs. 14 and 15 enable a different perspective of each array emission. While in this simulation, an interpenetrating monopole array has fewer energy-wasting emission peaks than a patch array of the same order, the main lobe gain for the former is less than the main lobe gain of the latter by approximately 2.5 dB.

Table 1 compares the total directivity gains of the principal emission emanating from an 8×8 phased array of patch radiators and an 8×8 array of 3×3 sub-arrays comprising 1/4 wave rod monopoles.

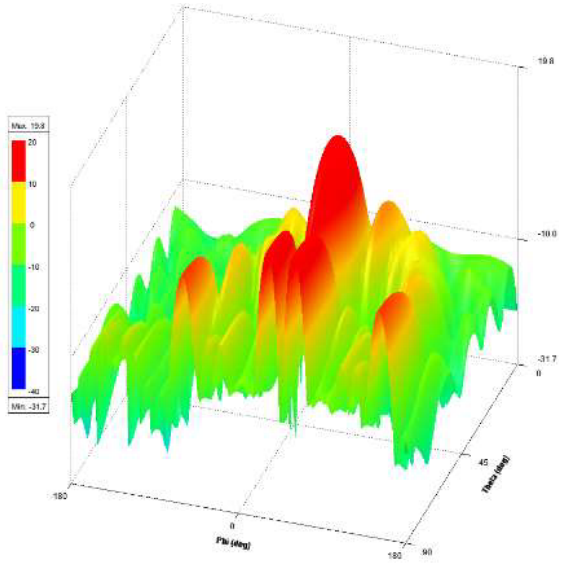

Figure 14. Rectangular plot of the directivity gain of the $(3 \times 3) \times (8 \times 8)$ array comprised of Inner Edge Activated monopole radiators with 45° Elevation and 45° Azimuth.

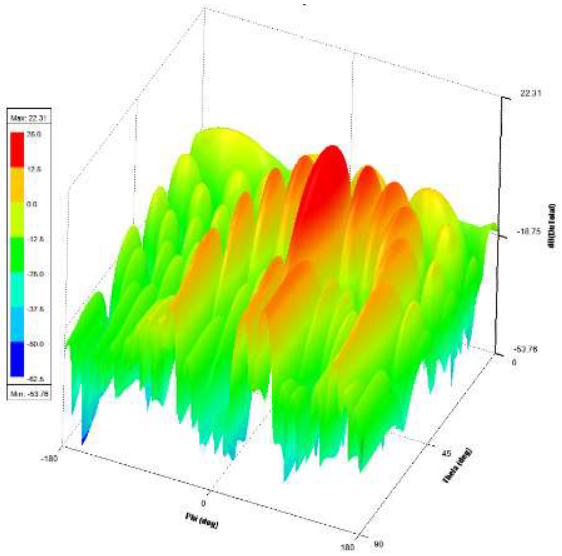

Figure 15. Rectangular plot of the directivity gain of the (8×8) array of patch radiators described in Fig. 11, with 45° Elevation and 45° Azimuth.

Table 1. Total directivity gain comparison between patch and monopole arrays of the same order.

Main Beam Angle (Elevation, Azimuth) (°)	Patch (dB)	$(3 \times 3) \times (8 \times 8)$ Center-Driven (dB)	$(3 \times 3) \times (8 \times 8)$ Inner Edge Driven (dB)	$(3 \times 3) \times (8 \times 8)$ Outer Edge Driven (dB)
(15, 15)	23.8	18.1	17.8	19.3
(45, 45)	19.9	20.0	19.8	20.4
(60, 45)	18.9	18.5	18.8	18.6

The working frequency is 30 GHz. The emission patterns in the cases of (elevation, azimuthal) angles (60°, 45°) are not shown but will be discussed in the Conclusion.

5. APPENDIX

Here we briefly address three questions: 1) mutual coupling among in-band monopole radiators, 2) coupling between mutually band-exclusive monopole radiators, and 3) coupling of active radiators to unterminated or floating radiators used in the simulations reported here.

1) For an array of rod monopoles, it is shown in [4] that the in-plane electric currents Jx and Jy and all magnetic currents vanish, leaving only the electric currents Jz in the evaluation of the transmitting and receiving coupling matrices. The cancellation of in-plane currents greatly simplifies estimating the direction of arrival, as is intuitively evident by the cylindrical symmetry of each radiator in the array.

2) Lack of induced currents by mutual coupling is also reasonably expected in the case of interpenetrating arrays that are spectrally separated by "impenetrable" guard bands because while EMFs are induced from out-of-band activity, the return path to ground is blocked by the "impenetrable" guard bands, and there are no induced flows of electric currents. The out-of-band monopoles are "floating" wires.

3) In the case of coupling between active and unterminated rod radiators, pertinent to the simulations reported here, it is clear that no energy can flow from the active to the unterminated

floating monopole as there is no return path to ground. The unterminated monopoles are just floating wires.

6. PROTOTYPE FABRICATION BASED ON 2.5D INTEGRATION

Prototype fabrication may be based on a modified 2.5D foundry integration for the phase shift control layer and a modified plastic pin grid array process for fabricating the 1/4 wavelength monopole air interface.

As depicted in Fig. 16, a generic array of 1/4 wave rod "monopoles" may be mounted above a current return plane. Uplink and downlink signals to the monopole array may be directed, in part, by the wiring redistribution layers RDL2 and RDL1 through a "Passive Interposer." Phase shifting control over the monopole array may occur in the "Phase Shift Layer" which may comprise, in part, 30 GHz 5-bit Digital phase shifters based on monolithic microwave integrated circuits. See, for example: https://www.qorvo.com/products/p/TGP2100.

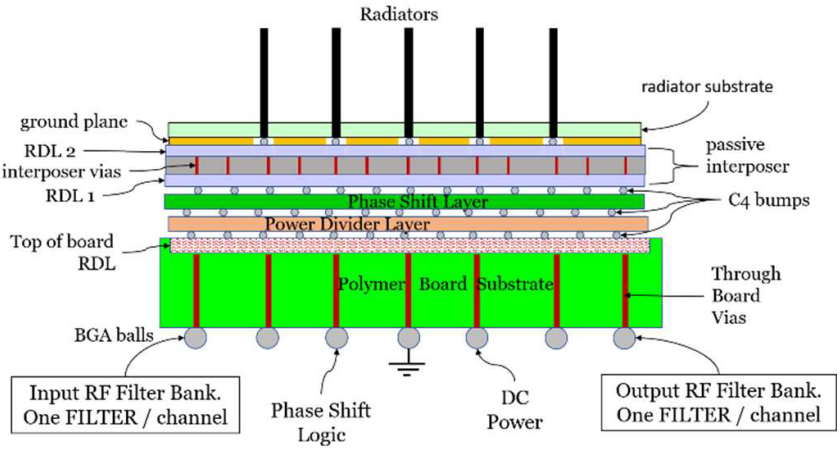

Figure 16. Cross sectional sketch of a 2.5D component stack-up process leading to an initial testable prototype.

A "Polymer Package Substrate" with a "Top of board RDL," provides mechanical support and electrical connections by means of "BGA balls," "Through Board Vias," C4 bumps, and an interposer with top and bottom wiring redistribution layers, RDL1 and RDL2. An input signal from an "Input Band" for each of the interpenetrating arrays is filtered through an "Input Filter Bank" containing one narrow bandpass filter "NBPF" for each channel, with roll-off of about 50 dB/MHz, for example, https://www.pasternack.jp/images/ProductPDF/PE-W42F004.pdf tuned to the center frequency of each channel. Similarly, a received signal is first filtered through a corresponding "Output Filter Bank" containing one narrow bandpass filter "NBPF" tuned to each receiving channel.

While this work was initially intended to provide highly enhanced throughput at outdoor base station phased array panels, it has since become clear that smaller versions of the concept may offer a more accessible introductory test market aimed at indoor/outdoor events such as conventions, technology fairs, and trade shows. Examples of small formfactor, millimeter wave, indoor base stations:

- (1×1) monopole per unit cell x (4×4) unit cells = two (4×4) interpenetrating phased arrays; 2 channels.
- (2×2) monopoles per unit cell x (4×4) unit cells = four (4×4) interpenetrating phased arrays; 4 channels.
- (3×3) monopoles per unit cell x (4×4) unit cells = nine 4×4 interpenetrating phased arrays; 9 channels.

Multiple channels and broad spatial coverage base stations with low antenna gain may be suited for indoor work-spaces with a large number of remote or in-person desk-top or floor-plan work stations.

In addition:

- CubeSat new missions will require higher data rates in the S-band, close to 3 GHz [3, 5]. This will require antenna arrays for directional gain. Patch radiator arrays can only provide one channel, whereas arrays of $(N \times N)$ monopole sub-arrays are able to provide multiple channels in the same patch array area.
- Further, to the best of our knowledge of the published literature and Letters Patents, large arrays of vertical rod monopoles have been reported only in applications of "over the horizon" RADAR arrays [6–8].

7. CONCLUSIONS

We have presented a new concept with which the throughput of large outdoor and small indoor wireless base stations is substantially enhanced based on high aspect ratio radiators being closely packed into sub-arrays from which, in turn, a number of sub-arrays can be arranged into interpenetrating, independent beamforming arrays such that when each interpenetrating array is spectrally isolated by guard bands, as may be facilitated by narrow bandpass filters, each independent beamformer will function as an independent beamformer for its designed channel center frequency and bandwidth. Thus, we have shown how to achieve at least a nine-fold channel diversity with nine monopoles per sub-array unit cell, resulting in nine independent phased arrays within the formfactor of a single array of an equal number of patch radiators.

By HFSS simulation we have shown that each interpenetrating array is agnostic with respect to its provenance in the sub-array. In addition, as seen in Table 1, the higher directivity gain attainable at small angles by a patch array is dissipated at larger elevations. Extrapolating from Table 1, the operational range of elevations over which a patch array gain and a monopole array gain are comparable is between 10° and 50° of elevation. As the angle of elevation increases to 60° for either a monopole or patch array of the same order, the directivity gain plot increases normally up to an elevation of about 55° and remains virtually unchanged at about 18.6 dB to 90°.

It is noted that using only patch arrays, a nine-fold increase in throughput can only be achieved by using nine independent patch arrays with a commensurate nine-fold increase in the panel size.

ACKNOWLEDGMENT

This work was supported, in part, by a no-cost extension of NSF award 1821819.

REFERENCES

1. Aburakhia, S. A., E. F. Badran, and D. A. Mohamed, "Distribution of the PAPR for real-valued OFDM signals," *4th International Conference on Information Technology (ICIT 2009)*, Al-Zaytoonah University, Jordon, June 2009, doi: 10.13140/2.1.1212.7680.
2. Mallik, R. K. and R. Murch, "Exact expressions for PAPR statistics in low number subcarrier multicarrier systems," *IEEE Wireless Communications Letters*, Vol. 9, 930–942, 2020, doi: 10.1109/LWC.2020.2974720.
3. Abulgasem, S., F. Tubbal, R. Raad, P. I. Theoharis, S. Lu, and S. Iranmanesh, "Antenna designs for CubeSats: A review," *IEEE Access*, Vol. 9, 45289–45324, 2021, doi: 10.1109/ACCESS.2021.3066632.
4. Henault, S. and Y. M. M. Antar, "Unifying the theory of mutual coupling compensation in antenna arrays," *IEEE Antennas and Propagation Magazine*, Vol. 57, 104–122, 2015, doi: 10.1109/MAP.2015.2414514.
5. Saeed, N., A. Elzanaty, H. Almorad, H. Dahrouj, T. Y. Al-Naffouri, and M.-S. Alouini, "CubeSat communications: Recent advances and future challenges," *IEEE Communications Surveys & Tutorials*, Vol. 22, 1839–1862, 2020, doi: 10.1109/COMST.2020.2990499.
6. Henault, S., "Analysis of planar array of 64 monopoles for over-the-horizon radar," Scientific Report DRDC-RDDC-2018-R233, Defence Research and Development Canada, January 2019.

7. Henault, S., "Analysis of planar array of 256 monopoles for over-the-horizon radar," Scientific Report DRDC-RDDC-2020-R123, Defence Research and Development Canada, November 2020.
8. Henault, S., "Improving auroral clutter rejection robustness in over-the-horizon radar," *2018 18th International Symposium on Antenna Technology and Applied Electromagnetics (ANTEM)*, 2018, doi: 10.1109/ANTEM.2018.8573001.